Monthly Notices
of the
ROYAL ASTRONOMICAL SOCIETY

MNRAS **488,** 4585–4595 (2019)
Advance Access publication 2019 July 26

doi:10.1093/mnras/stz1992

How low does it go? Too few Galactic satellites with standard reionization quenching

Andrew S. Graus,[1,2]★ James S. Bullock,[1] Tyler Kelley,[1] Michael Boylan-Kolchin,[2] Shea Garrison-Kimmel[3] and Yuewen Qi[1]

[1]*Center for Cosmology, Department of Physics and Astronomy, 4129 Reines Hall, University of California Irvine, CA 92697, USA*
[2]*The University of Texas at Austin, Department of Astronomy, 2515 Speedway, Stop C1400, Austin, TX 78712, USA*
[3]*TAPIR, Mailcode 350-17, California Institute of Technology, Pasadena, CA 91125, USA*

Accepted 2019 July 17. Received 2019 July 16; in original form 2018 August 10

ABSTRACT

A standard prediction of galaxy formation theory is that the ionizing background suppresses galaxy formation in haloes with peak circular velocities smaller than $V_{\rm peak} \simeq 20\,{\rm km\,s^{-1}}$, rendering the majority of haloes below this scale completely dark. We use a suite of cosmological zoom simulations of Milky Way-like haloes that include central Milky Way disc galaxy potentials to investigate the relationship between subhaloes and ultrafaint galaxies. We find that there are far too few subhaloes within 50 kpc of the Milky Way that had $V_{\rm peak} \gtrsim 20\,{\rm km\,s^{-1}}$ to account for the number of ultrafaint galaxies already known within that volume today. In order to match the observed count, we must populate subhaloes down to $V_{\rm peak} \simeq 6\,{\rm km\,s^{-1}}$ with ultrafaint dwarfs. The required haloes have peak virial temperatures as low as 1500 K, well below the atomic hydrogen cooling limit of 10^4 K. Allowing for the possibility that the Large Magellanic Cloud contributes several of the satellites within 50 kpc could potentially raise this threshold to $10\,{\rm km\,s^{-1}}$ (4000 K), still below the atomic cooling limit and far below the nominal reionization threshold.

Key words: galaxies: dwarf – galaxies: formation – (galaxies:) Local Group – cosmology: theory – (cosmology:) dark ages, reionization, first stars.

1 INTRODUCTION

One of the foundational developments in near-field cosmology was the discovery of ultrafaint dwarf galaxies in the Sloan Digital Sky Survey (SDSS; see Willman 2010 for a review). More recent efforts from Dark Energy Survey (DES), PanSTARRS, and MagLiteS (among other surveys) have led to many additional discoveries of ultrafaint Milky Way satellites (Drlica-Wagner et al. 2015; Koposov et al. 2015; Laevens et al. 2015a, b; Drlica-Wagner et al. 2016); the current census of ultrafaint satellites in the Milky Way is approximately 45. These galaxies are incredibly faint, with luminosities as low as $\sim 350\,{\rm L_\odot}$, and heavily dark matter dominated (Simon & Geha 2007). As such, they may represent the long-discussed 'Missing Satellites' of the Milky Way (Klypin et al. 1999; Moore et al. 1999). We expect many more such objects to exist within the virial radius of the Milky Way; only about half the sky has been surveyed and is only complete to within ∼30 kpc for the faintest dwarfs (Walsh, Jerjen & Willman 2007).

The stars in all ultrafaint galaxies are universally old ($\gtrsim 11$ Gyr) and this lends credence to the idea that their star formation was shut down in response to reionization at high redshift (Bovill & Ricotti 2009; Brown et al. 2014; Weisz et al. 2014; Wheeler et al. 2015). While most of these ancient ultrafaint dwarfs are satellites of larger systems, it is statistically unlikely that environmental quenching could have quenched star formation early enough in these objects to explain the absence of young stars in all of them (Rodriguez Wimberly et al. 2019).

Reionization suppression is an attractive mechanism for explaining the uniformly ancient stellar populations of ultrafaint dwarfs, as there should be a dark matter halo mass scale below which galaxy formation is severely limited by the ionizing background (Efstathiou 1992). The majority of models that have explored the reionization suppression scale have found that most dark matter haloes with peak maximum circular velocities ($V_{\rm peak}$) smaller than $V_{\rm peak} \simeq 20$–$30\,{\rm km\,s^{-1}}$ are unable to accrete gas after reionization (Thoul & Weinberg 1996; Gnedin 2000; Hoeft et al. 2006; Okamoto, Gao & Theuns 2008). This is not unexpected, as haloes of this size have virial temperatures of $T_{\rm vir} \sim 20\,000$ K, which is similar to the IGM temperature after reionization (e.g. McQuinn 2016; Oñorbe, Hennawi & Lukić 2017). Suppression at this scale also naturally solves the missing (classical) satellites problem (Bullock,

★ E-mail: agraus@utexas.edu

Kravtsov & Weinberg 2000; Benson et al. 2002; Somerville 2002; Kim, Peter & Hargis 2018; Read & Erkal 2018).

More recently, Ocvirk et al. (2016) have used full radiative transfer simulations of the Local Group to show that reionization suppresses galaxy formation in haloes with $M_{\rm vir} \simeq 5 \times 10^8$ $M_\odot$ measured at $z = 5.5$, which is equivalent to $V_{\rm max} \simeq 20$–25 km s^{-1} at this redshift.[1] A similar quenching threshold is seen in high-resolution hydrodynamic simulations that track dwarf galaxy formation down to redshift zero (Sawala et al. 2016; Benítez-Llambay et al. 2017; Fitts et al. 2017; Macciò et al. 2017; Munshi et al. 2017). For example, Fitts et al. (2017) have used FIRE zoom simulations to study dwarf galaxy formation and find that the majority of haloes with peak subhalo masses below 10^9 $M_\odot$ form no stars. This is equivalent to a threshold at $V_{\rm peak} \simeq 20$ km s^{-1}.

A second scale of relevance for low-mass galaxy formation is the atomic hydrogen cooling limit at 10^4 K, which corresponds to a $V_{\rm peak} \simeq 16$ km s^{-1} halo. Systems smaller than this would require molecular cooling to form stars. Taken together, one might expect that most ultrafaint satellite galaxies of the Milky Way should reside within subhaloes that fell in with peak circular velocities in the range 16–30 km s^{-1}, though these systems would have lower maximum circular velocities ($V_{\rm max}$) *today* as a result of dark matter mass-loss after infall on to the Milky Way's halo ($V_{\rm max} \leq V_{\rm peak}$).

In addition to tidal stripping, the destruction of dark matter subhaloes due to interactions with the potential of the central galaxy itself is a crucial physical process that must be included in any comparison to satellite galaxy counts (D'Onghia et al. 2010; Brooks & Zolotov 2014; Wetzel et al. 2016; Zhu et al. 2016; Garrison-Kimmel et al. 2017). The effect of the central galaxy decreases subhalo abundances by about a factor of two within the virial radius compared to dark matter only simulations; a similar effect is seen in massive elliptical galaxy haloes (Despali & Vegetti 2017; Graus et al. 2018). The enhanced destruction is particularly important for subhaloes close to the central galaxy. At the Milky Way scale, almost all haloes above the resolution limit are destroyed within 20 kpc (Garrison-Kimmel et al. 2017). This level of depletion, combined with the pace of new discoveries at small Galacto-centric radii, leads us to ask whether there may be *too many* Milky Way satellites rather than not enough (see e.g. Jethwa, Erkal & Belokurov 2018; Li, Gao & Wang 2019).

In this work, we use a new suite of cosmological zoom simulations of Milky Way-like haloes simulated with an evolving Milky Way disc (plus bulge) potential to explore the relationship between dark matter haloes and ultrafaint galaxies. We show that a conventional reionization suppression scale at $V_{\rm peak} \simeq 20$ km s^{-1} drastically underproduces the count of Milky Way satellites within 50 kpc of the Galactic Centre. Assuming the Milky Way is typical of our simulation suite, it appears that a significant fraction of ultrafaint galaxies must form in subhaloes with peak circular velocities less than 10 km s^{-1}. These haloes have virial temperatures of $T_{\rm vir} < 4000$ K, which is well below the nominal atomic hydrogen cooling limit. In Section 2, we describe the simulations. Section 3 presents our results. Section 4 discusses some possibilities that could alter our conclusions, and Section 5 provides a summary discussion.

[1]Note that $V_{\rm vir} \propto (1+z)^{1/2}$ at fixed halo mass if we ignore the potential (mild) evolution in the virial overdensity definition.

2 SIMULATIONS AND METHODS

In this work, we use a new zoom simulation suite performed by Kelley et al. (2019) that consists of dark matter only Milky Way-like haloes simulated with a disc+bulge potential to account for the destructive effects of the central galaxy. The galaxy potentials were implemented in a manner similar to that discussed in Garrison-Kimmel et al. (2017), who showed that this approach mimics the enhanced subhalo destruction seen in full hydrodynamic simulations.

The simulations were run with GIZMO (Hopkins 2015), which uses an updated version of the TREE+PM gravity solver from GADGET-3 (Springel 2005). The simulations have a force softening length of 25 pc h^{-1} and a high-resolution dark matter particle mass of 2×10^4 $M_\odot$ h^{-1}. This corresponds to a resolved subhalo maximum circular velocity $V_{\rm max} = 4.5$ km s^{-1}. All of the simulations are cosmological zoom-in simulations (Katz & White 1993; Oñorbe et al. 2014) with initial conditions generated by MUSIC (Hahn & Abel 2011), assuming a box size of 50 Mpc h^{-1}, and a cosmology from Planck (2016): $h = 0.6751$, $\Omega_\Lambda = 0.6879$, and $\Omega_{\rm m} = 0.3156$.

The host haloes in these simulations were selected to have halo masses at $z = 0$ of $M_{\rm vir} = 0.8$–2×10^{12} $M_\odot$, in line with current estimates of the Milky Way halo mass. These haloes are also isolated such that they are the largest halo within 3 Mpc. The suite consists of 12 haloes run both with and without the disc implementation for a total of 24 simulations.

While a basic description of how the disc is implemented in the code can be found in Garrison-Kimmel et al. (2017), several modifications have been made to the properties of the galaxy potential in order to match precisely the Milky Way and its expected evolution. Specifically, we mimic an exponential disc galaxy potential following Smith et al. (2015), who show that three summed Miyamoto–Nagai discs (Miyamoto & Nagai 1975) provide a good approximation to an exponential disc. We use this method to model the gas and stellar discs of the Milky Way. We further include the bulge of the Milky Way as a Hernquist potential (Hernquist 1990).

The $z = 0$ values for the properties of the Milky Way bulge, stellar, and gas discs (including both masses and scale heights) were taken from Bland-Hawthorn & Gerhard (2016) and McMillan (2017). The disc is initialized at $z = 3$, and the time evolution of the stellar mass is determined by tying the stellar-mass growth to the halo mass growth using abundance matching from Behroozi, Wechsler & Wu (2013). The evolution of the scale radii is then matched to CANDELS data from van der Wel et al. (2014). The gas mass is tied to the evolution of the cold gas fraction seen from CANDELS (Popping et al. 2015), and the gas scale radius is fixed to be a constant multiple of the (time-evolving) stellar disc scale radius. Finally, the bulge is modelled with a mass and scale radius fixed to that of the stellar disc so that the ratios are a constant as a function of time. A full description of the suite of simulations along with basic properties of their satellites will be given in Kelley et al. (2019).

3 SUBHALO COUNTS AND DISTRIBUTIONS

Fig. 1 presents $V_{\rm peak}$ functions for subhaloes within 300 kpc of each host; $V_{\rm peak}$ is defined as the maximum of $V_{\rm max}$ over all time, which is usually reached prior to subhalo infall at a distance of 1.5–7 virial radii from the host (Behroozi et al. 2014). The shaded bands correspond to the full width of the distributions

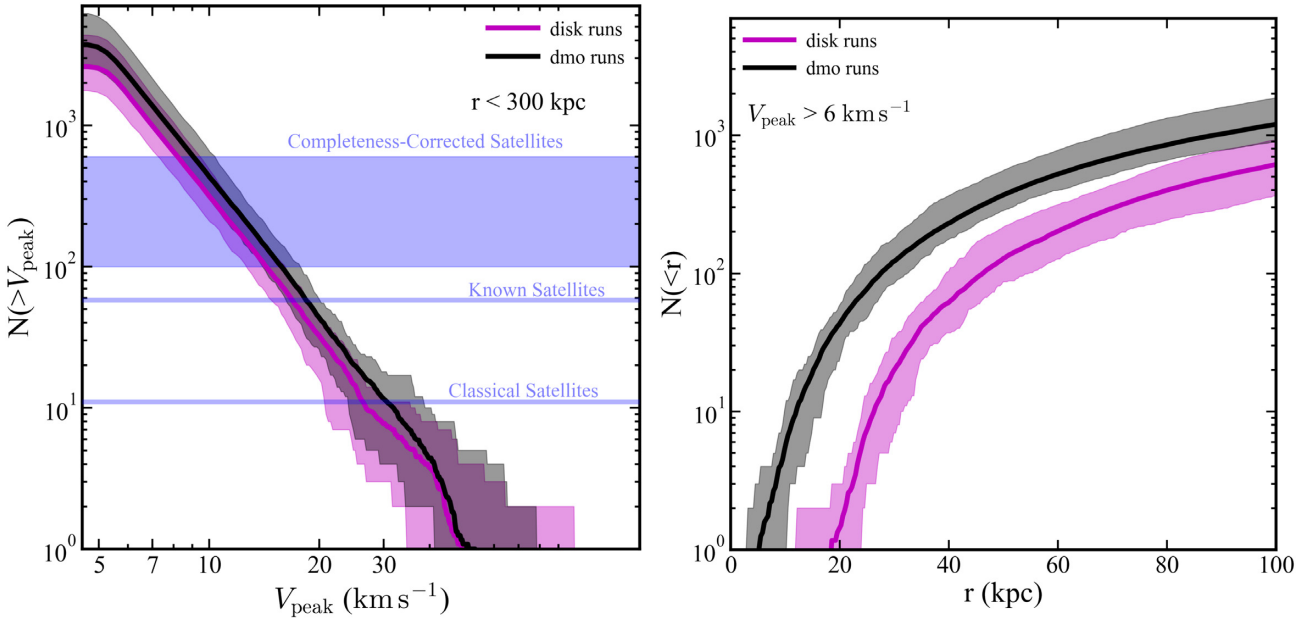

Figure 1. *Left:* Cumulative subhalo counts within 300 kpc as a function of the peak maximum circular velocity achieved over subhalo's history, $V_{\rm peak}$. The black distribution represents the full range of our dark matter only simulations, while the magenta distribution represents the simulations with analytic disc potentials. The solid lines are medians. The horizontal lines show the number of classical satellites. All presently known satellites, and the range of total satellites expected based on sky and volume completeness corrections. *Right:* Radial distribution of all subhaloes with $V_{\rm peak} \geq 6\,{\rm km\,s^{-1}}$ for the dmo simulations (black) and the dmo+disc simulations (magenta).

over all simulations. Compared to the dark matter only (dmo) simulations (black), the disc simulations (magenta) show a factor of ~ 50 per cent less substructure within this volume (consistent with Garrison-Kimmel et al. 2017). Both sets of simulations begin to flatten at $V_{\rm peak} \simeq 6\,{\rm km\,s^{-1}}$, which we take as our completeness limit. As mentioned above, we are complete to current maximum circular velocities of $V_{\rm max} \simeq 4.5\,{\rm km\,s^{-1}}$.

The horizontal lines in Fig. 1 show the number of classical Milky Way satellites and the current count of all satellite galaxies known. The band shows a range of estimates[2] for the total number of satellite galaxies after accounting for incompleteness and sky coverage limits (Tollerud et al. 2008; Kim et al. 2018; Newton et al. 2018). We see that, based on counts, the classical satellites are consistent with sitting in haloes with $V_{\rm peak} \geq 30\,{\rm km\,s^{-1}}$. The range of completeness-corrected satellites corresponds to $V_{\rm peak}$ between 8 and 18 $\rm km\,s^{-1}$. The lower end of estimates ($\sim$100) is more in line with the standard expectation for reionization quenching at $V_{\rm peak} \simeq 20\,{\rm km\,s^{-1}}$. The upper end of the range ($\sim$600) would suggest the need to populate quite small haloes $V_{\rm peak} \simeq 8\,{\rm km\,s^{-1}}$, well below the atomic cooling limit.

As shown by Garrison-Kimmel et al. (2017), disc destruction is particularly important at small radii. In the right-hand panel of Fig. 1, we show the radial distribution of satellites with $V_{\rm peak} > 6\,{\rm km\,s^{-1}}$ out to 100 kpc for both the dmo and dmo+disc simulations. As before, the bands show the full width over all simulations and the solid lines show the medians. The disc simulations retain very little substructure within 20 kpc.

The vast majority of subhaloes have $z_{\rm peak} \leq 3$ (97 per cent in the disc simulations and 93 per cent in the dmo simulations). The average $z_{\rm peak}$ for surviving subhaloes within 50 kpc is $\langle z_{\rm peak} \rangle = 0.77$ for the disc runs and $\langle z_{\rm peak} \rangle = 0.94$ for the dmo runs. This difference is due to the enhanced subhalo destruction caused by the disc, which preferentially destroys subhaloes that fall in early (Kelley et al. 2019).

Fig. 2 shows only the (more realistic) disc simulations, now restricted to the inner 100 kpc. The three bands show radial distribution of subhaloes with $V_{\rm peak} > 6$, 10, and 18 $\rm km\,s^{-1}$. Note that there are typically no subhaloes with $V_{\rm peak} > 18\,{\rm km\,s^{-1}}$ that survive within 40 kpc. This is surprising given that we certainly know of satellite galaxies within 40 kpc of the Milky Way, and $V_{\rm peak} \simeq 18\,{\rm km\,s^{-1}}$ is close to the conventional scale for reionization suppression where haloes begin to go dark.

The black dashed line shows the radial distribution of known satellite galaxies out to 100 kpc. We know the census of satellites is incomplete both radially (due to luminosity incompleteness) and in area on the sky (less than $\sim$1/2 of the sky has been covered in searches capable of finding ultrafaint galaxies). Nevertheless, the total count of satellite galaxies exceeds the median subhalo count at small radius for all but the $V_{\rm peak} > 6\,{\rm km\,s^{-1}}$ sample (red). The $V_{\rm peak} > 18\,{\rm km\,s^{-1}}$ distribution, which is closest to the canonical reionization suppression scale, drastically underpredicts the number of known galaxies (see Newton et al. 2018 for a list of galaxies within $R_{\rm vir}$).

Fig. 2 demonstrates that in order to account for the satellite galaxies of the Milky Way that are known to exist within $\sim$30 kpc, we need to resort to populating haloes with $V_{\rm peak}$ values that are substantially lower than canonical values for reionization quenching that have been discussed in the literature. These counts are known to

[2]These completeness corrections typically assume the radial distribution of satellites follows results of dmo simulations. Such corrections are often calculated by calculating the ratio of observed galaxies in a survey volume to simulated subhaloes in a similar volume. Then applying that correction to the total number of subhaloes around the Milky Way. In simulations of disc disruption, the number of subhaloes in the mock survey volume will decrease, increasing the overall correction. In this sense, the corrections shown here are conservatively low.

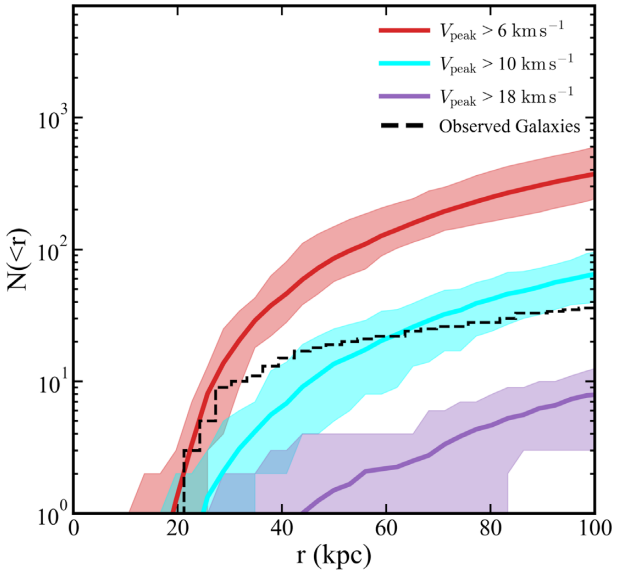

Figure 2. Radial distributions of subhaloes with $V_{peak} > 6$, 10, and 18 km s^{-1} in the disc runs. The dashed line shows the radial distribution of known satellite galaxies, which is lower limit on the total. Half of the sky has not been surveyed for ultrafaint dwarfs and the other half is incomplete at radii beyond ∼30 kpc. Still, the current satellite census is above the median subhalo counts at small radius unless we associate galaxies with the smallest subhaloes we resolve $V_{peak} > 6\,km\,s^{-1}$. The nominal reionization threshold would lead to an expectation close to the 18 km s^{-1} line (purple), which is far below the data.

be significantly incomplete at larger radius even in areas of the sky that have been covered by surveys like SDSS and DES. Below, we present a somewhat more detailed exploration of what the ultrafaint Milky Way satellite population tells us about the low-mass threshold of galaxy formation.

3.1 Satellite occupation fractions

Simulations that have explored how haloes go dark at low masses typically find that the fraction of haloes hosting a galaxy of any mass (f_{galaxy}) drops towards zero smoothly below a characteristic value of V_{peak} (e.g. Sawala et al. 2016; Fitts et al. 2018). In order to allow for this expectation, we have explored a toy model where the fraction of haloes that host a galaxy of any mass varies smoothly from zero at small V_{peak} to unity as V_{peak} increases. We specifically adopt a cumulative Gaussian, which allows for a characteristic scale (V_{50}) where 50 per cent of haloes become dark and a width (σ) that sets the sharpness of the transition from dark haloes to galaxy-hosting haloes:

$$f_{galaxy}(> V_{peak}) = \frac{1}{2}\left[1 + \mathrm{erf}\left(\frac{V_{peak} - V_{50}}{\sqrt{2}\sigma}\right)\right]. \quad (1)$$

The upper left-hand panel of Fig. 3 shows two models of this kind along with a simple threshold model (red) for comparison. The blue line shows a conventional model with $V_{50} = 18\,km\,s^{-1}$ and $\sigma = 2.5$. These values are chosen to match the FIRE-2 results presented in Fitts et al. (2018), but they are typical of other results in the literature: haloes begin to go dark at $V_{peak} \simeq 25\,km\,s^{-1}$ and go completely dark by $V_{peak} \simeq 10\,km\,s^{-1}$. A case that shifts the quenching scale a factor of ∼3 lower in virial temperature is shown in yellow: $V_{50} = 10.5\,km\,s^{-1}$ with $\sigma = 2.5$.

In order to compare the predictions of these simple models to the observed population of Milky Way satellites, we take into account sky coverage completeness and account for the fact that subhalo populations are anisotropic. We restrict ourselves to only satellites within either the SDSS or DES footprints, both of which have well-defined completeness areas. We make no allowance for luminosity/volume incompleteness in order to be conservative. Using equation (1) we assign a galaxy to each subhalo probabilistically for all 12 of our disc simulations; and repeat this procedure 100 times counting 'galaxies' as a function of radius within mock survey areas. The SDSS and DES survey regions are approximated as three cones with the areas of the two contiguous SDSS fields and the DES field, and their orientations are fixed relative to one another to match the surveys. Each iteration uses a different orientation of the cones. Note that unlike the real DES and SDSS fields, we orient the survey cones randomly with respect to the disc planes. We do this because it increases our statistics and because we find that the disc does not introduce any significant asymmetry. In fact, it sphericalizes the subhalo distributions compared to the dmo runs (Garrison-Kimmel et al. 2017; Kelley et al. 2019; Riley et al. 2018)

The top right-hand panel in Fig. 3 shows the results of this exercise for our simple $V_{peak} \geq 6\,km\,s^{-1}$ threshold model. The shaded band includes the full scatter over all simulations and survey orientations, with the solid line showing the average. The bottom left-hand and bottom right-hand panels show the full distributions (minimum and maximum) of the $V_{50} = 10.5\,km\,s^{-1}$ and $V_{50} = 18\,km\,s^{-1}$ models, respectively. For comparison, the galaxies in SDSS and DES are shown as a black histogram. Table 1 lists all satellite galaxies within 50 kpc of the Milky Way. We include only the satellites that sit within the SDSS or DES footprints[3] in Fig. 3. The current census is incomplete at large radius so the dashed lines in Fig. 3 are lower limits.

As is clear from Fig. 3, the $V_{peak} \geq 6\,km\,s^{-1}$ model matches the observed distribution the best at small radius (where incompleteness matters least). This is surprising since these haloes are far lower mass than those naively expected to host galaxies. In contrast, the most well-motivated model, with $V_{50} = 18\,km\,s^{-1}$, fails to form enough galaxies in the inner regions to match the number of galaxies already observed. In fact, the average is less than one galaxy out to 50 kpc. The $V_{50} = 10.5\,km\,s^{-1}$ model produces a distribution that is consistent with the observed counts, primarily because it has a tail of non-zero occupation that stretches down to low-mass haloes.

Another way to see how surprisingly low mass the required haloes are is to look at the distribution of virial temperatures for the haloes in these models. For this, we use

$$T_{vir} \simeq 10^4 K \left(\frac{V_{peak}}{16.3\,km\,s^{-1}}\right)^2, \quad (2)$$

which follows from $T_{vir} = \mu m_p c_g^2/k_b$ with $c_g = V_{max}/\sqrt{2}$ and $\mu = 0.62$, as implied by a 30 per cent mass fraction in helium.[4] The left-hand panel of Fig. 4 shows the T_{vir} distribution for the galaxy-populated subhaloes within 50 kpc for each of the three models

[3]Currently, we know of about 58 satellites around the Milky Way; however, this includes many candidate ultrafaint galaxies from surveys such as DES, MagLiteS, and PanSTARRS that have yet to be spectroscopically confirmed.
[4]In the original definition of T_{vir}, $c_g = V_{vir}/\sqrt{2}$, we have replaced V_{vir} with V_{max} as it is an upper limit on the virial temperature. As the point of this exercise is to point out how much lower the T_{vir} is than the atomic cooling limit, any decrease in the assumed velocity will only strengthen this discrepancy.

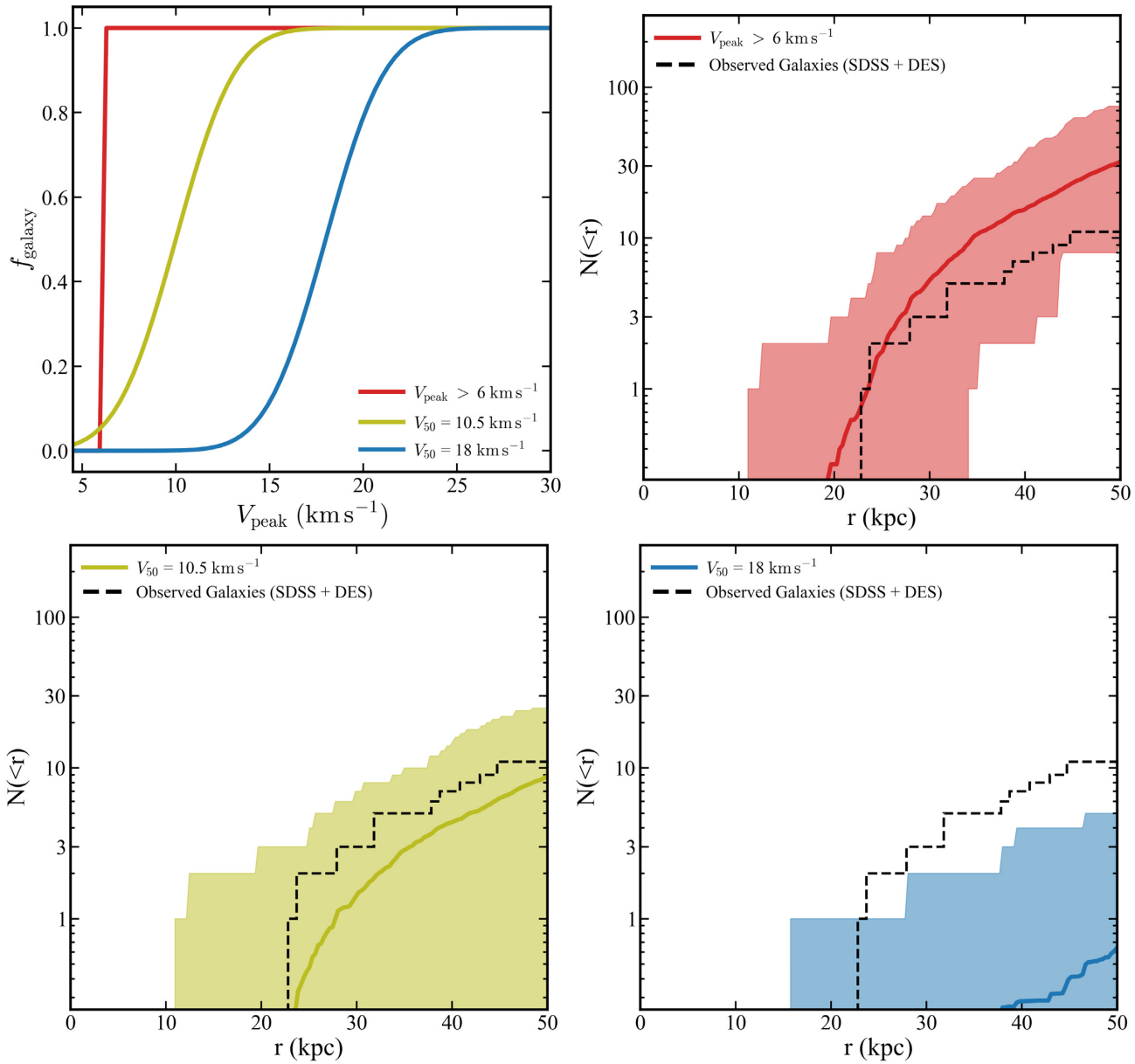

Figure 3. *Top left*: The models used to calculate which haloes could potentially host a galaxy. The blue is a 'conventional' model based on estimates of the dark fraction from hydrodynamic simulations. The dashed black lines in the other panels show the radial distribution of Milky Way satellites restricted to those within the SDSS and DES regions. These distributions are almost certainly incomplete at large radius, and thus represent lower limits. *Top right*: The predicted radial distribution of satellites within the SDSS plus DES regions, assuming every halo with $V_{\rm peak} \geq 6\,{\rm km\,s^{-1}}$ forms a galaxy. *Bottom left*: The distribution after applying the $V_{50} = 10.5\,{\rm km\,s^{-1}}$ model. *Bottom right*: The distribution for the $V_{50} = 18\,{\rm km\,s^{-1}}$ model. The predicted distributions come from mock observations within angular regions that mimic SDSS and DES coverage. The bands thus represent the full halo-to-halo scatter and scatter from anisotropy in the distribution of subhaloes.

discussed in relation to Fig. 3. The two models that produce consistent Milky Way satellite populations all require that we populate subhaloes with $T_{\rm vir} < 4000$ K. This is well below the atomic cooling limit and the canonical reionization quenching scale.

What do the dark matter haloes of these galaxies look like today? The right-hand panel of Fig. 4 shows the distribution of $V_{\rm max}$ values (at $z = 0$) of the populated subhaloes in each of our three example models. Both of the consistent models (yellow and red) populate haloes with $V_{\rm max} \simeq 5$–$10\,{\rm km\,s^{-1}}$ today, with a small tail of maximum circular velocities out to $\sim 15\,{\rm km\,s^{-1}}$. While we cannot measure the maximum circular velocities of Milky Way dwarf satellites directly, we can measure the circular velocity at the half-light radius, $V_{\rm c}(r_{1/2})$. This represents a lower limit on the true $V_{\rm max}$ of the halo. Values of $V_{\rm c}(r_{1/2})$ for the Milky Way dwarfs within 50 kpc are listed in Table 1. Interestingly, of the 18 galaxies within 50 kpc (if surveys like MagLiteS and PanSTARRS are included) 3 have $V_{\rm c}(r_{1/2}) > 10\,{\rm km\,s^{-1}}$, which is already larger than typical $V_{\rm max}$ values in the successful models. The rest have circular velocities at $r_{1/2}$ that are at least consistent with those expected. Determining $V_{\rm max}$ estimates based on these measurements will require density

Table 1. Table of galaxies within 50 kpc of the Milky Way. Galaxies within the SDSS and DES footprints (with well-understood completeness areas) are listed above the solid line. Galaxies below the horizontal line are other galaxies known to exist within 50 kpc. We provide Galacto-centric radius, stellar velocity dispersion, implied circular velocity at the half-light radius, the half-light radius, and referenced for discovery and $\sigma_{\rm star}$. $V_{\rm c}(r_{1/2})$ is a lower limit on the current value of $V_{\rm max}$. Some distance and half-light radii measurements have been updated since discovery in which case we use the values provided by Simon (2019).

Name	$D_{\rm GC}$ (kpc)	$\sigma_{\rm star}$ (km s^{-1})	$V_{\rm c}(r_{1/2})$ (km s^{-1})	$r_{1/2}$ (pc)	Source	Disc ref.[a]	$\sigma_{\rm star}$ ref.[b]
Galaxy	(1)	(2)	(3)	(4)		–	
Segue I	23	$3.7^{+1.4}_{-1.4}$	6.4	24	SDSS DR6	(1)	(15)
DES J0225+0304	24	–	–	18.5	DES	(2)	–
Tucana III	25	$\leq$1.2	$\leq$2.1	37	DES	(3), (4)	(16)
Cetus II	30	–	–	17	DES	(3), (4)	–
Reticulum II	32	3.3 ± 0.7	5.7	51	DES	(3), (4)	(17)
Ursa Major II	35	5.6 ± 1.4	9.7	139	SDSS DR4	(5)	(18)
Segue II	37	$\leq$2.2	3.8	40	SDSS DR7	(6)	(19)
Boötes II	42	10.5 ± 7.4	18.2	39	SDSS DR5	(7)	(20)
Coma Berenices	42	4.6 ± 0.8	8.0	69	SDSS DR5	(1)	(18)
Willman I	45	4.0 ± 0.8	6.9	33	SDSS DR2	(8)	(21)
Tucana IV	48	–	–	127	DES	(3), (4)	–
Draco II	22	≤ 5.9	≤ 10.2	19	Pan-STARRS	(9)	(22)
Sagittarius I	27	9.6 ± 0.4	16.62	2662	Classical	(10)	(23)
Hydrus 1	28	$2.69^{+0.51}_{-0.43}$	4.7	53	DECam	(11)	–
Carina III	28	$5.6^{4.3}_{-2.1}$	9.7	30	MagLiteS	(12)	(24)
Triangulum II	28	≤ 3.4	≤ 5.9	16	Pan-STARRS	(13)	(25)
Carina II	36	$3.4^{+1.2}_{-0.8}$	5.89	92	MagLiteS	(12)	(24)
Pictor II	45	–	–	47	MagLiteS	(14)	–

[a](1) Belokurov et al. (2007), (2) Luque et al. (2017), (3) Drlica-Wagner et al. (2015), (4) Koposov et al. (2015), (5) Zucker et al. (2006), (6) Belokurov et al. (2009), (7) Walsh et al. (2007), (8) Willman et al. (2005), (9) Laevens et al. (2015a), (10) Ibata et al. (2014), (11) Koposov et al. (2018), (12) Torrealba et al. (2018), (13) Laevens et al. (2015b), (14) Drlica-Wagner et al. (2016).
[b](15) Simon et al. (2011), (16) Simon et al. (2017), (17) Simon et al. (2015), (18) Simon (2019), (19) Kirby et al. (2013), (20) Koch et al. (2009), (21) Willman et al. (2011), (22) Longeard et al. (2018), (23) Bellazzini et al. (2008), (24) Li et al. (2018a), (25) Kirby et al. (2017).

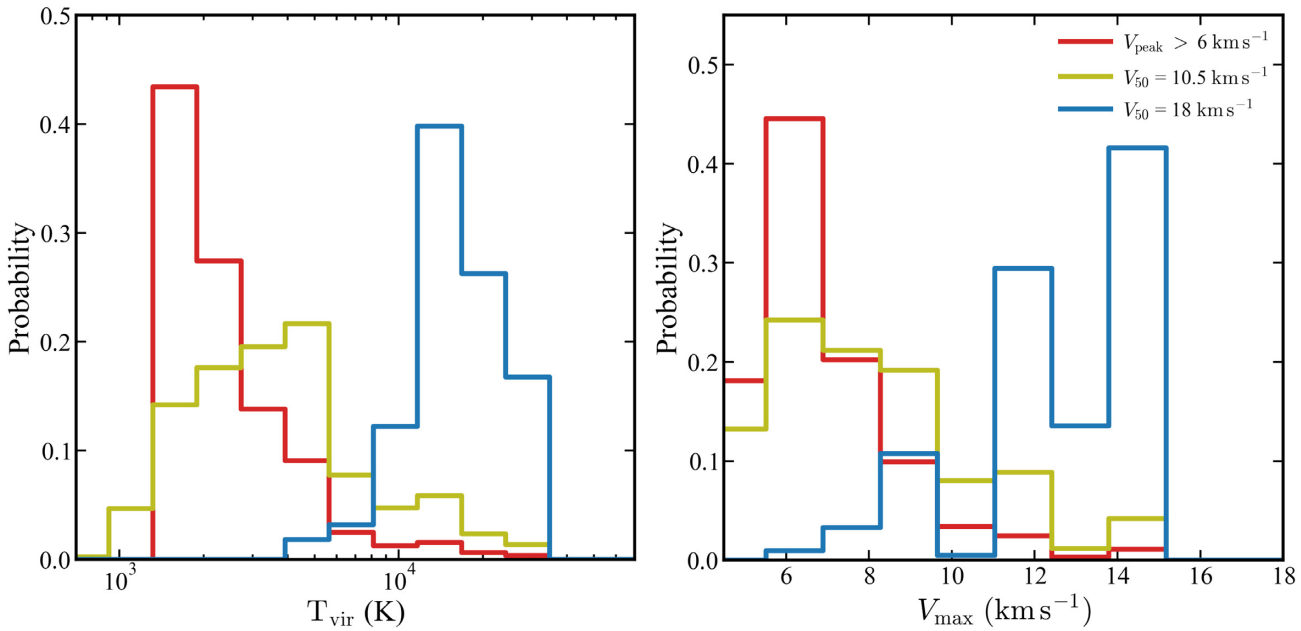

Figure 4. *Left:* The distribution of $T_{\rm vir}$ values for the suhaloes populated by galaxies in the models shown in Fig. 3. Recall that the $V_{50} = 18\,{\rm km\,s^{-1}}$ model (blue) drastically underpredicts Milky Way satellite counts, while the $V_{50} = 10.5\,{\rm km\,s^{-1}}$ (yellow) and $V_{\rm peak} > 6\,{\rm km\,s^{-1}}$ (red) models produce adequate counts. The consistent models all require galaxies to exist in haloes with virial temperatures of $\lesssim$4000 K, well below the atomic cooling limit. *Right:* The $V_{\rm max}$ distributions at $z = 0$ for subhaloes within 50 kpc of the Milky Way for the same models. The successful models peak below $7\,{\rm km\,s^{-1}}$ today.

profile priors to extrapolate from $r_{1/2}$ to the peak of the rotation curve at $r_{\rm max}$ (e.g. Boylan-Kolchin, Bullock & Kaplinghat 2011). Such an exploration is beyond the scope of this paper, but for context, a $V_{\rm max} \simeq 15\ {\rm km\,s^{-1}}$ ($7\ {\rm km\,s^{-1}}$) halo typically has $r_{\rm max} \simeq 1.5$ kpc (500 pc) (e.g. Garrison-Kimmel et al. 2014). This is a significant extrapolation for most ultrafaint dwarfs.

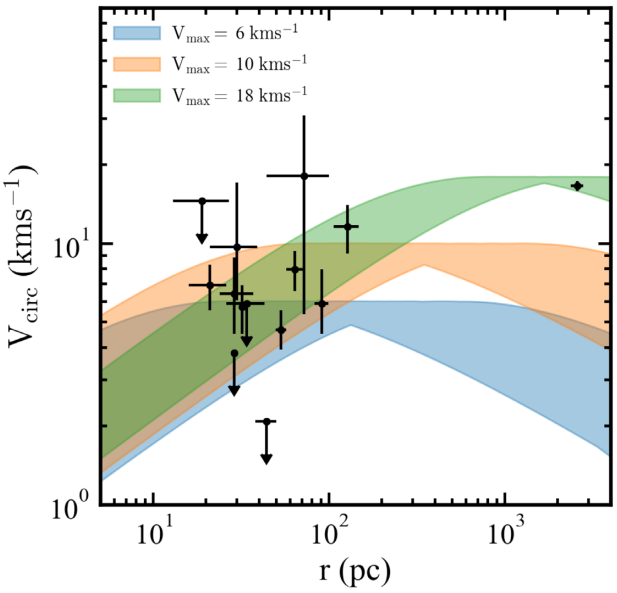

Figure 5. The circular velocity at the half-light radius $V_c(r_{1/2})$ for the galaxies within 50 kpc of the Milky Way, that have measured velocities (Table 1). For comparison, we also plot NFW profiles for haloes with V_{max} = 6, 10, 18 km s^{-1}. We can see that most of the galaxies within 50 kpc can be hosted by haloes with $V_{max} < 18$ km s^{-1} within errors. With notable exceptions being Sagittarius (which is clearly massive), and the lowest point Tucana III. Tucana III is interesting as it is shows evidence of being actively disrupted Li et al. (2018b).

Finally, we turn to whether or not haloes with the masses required to match the radial distribution of satellites can practically host the galaxies seen within 50 kpc. One way to do this is by estimating the circular velocities of the galaxies at the half-light radius. The circular velocities at the half-light radius for the galaxies within 50 kpc are listed in Table 1, and we plot the resulting data against the half-light radius with errors in Fig. 5. For comparison, we plot NFW circular velocity profiles for haloes at three masses (6, 10, and 18 km s^{-1}). The full distributions are derived by taking the 1σ distribution in concentrations from haloes at that mass from our simulation suite. One can see that most of the galaxies within 50 kpc can fit neatly into haloes of 6 and 10 km s^{-1}. The radius at which V_{max} is reached (R_{max}) for the dark matter haloes is large compared to the half-light radii of almost all the galaxies within 50 kpc, thus most of the galaxies can be hosted by a 6,10, or 18 km s^{-1} halo. However, it is also possible that these galaxies lie in haloes that were heavily stripped (Fattahi et al. 2018). Indeed, one of the few galaxies that cannot fit in any of the example NFW profiles is actually too low. This galaxy is Tucana III, which is interesting as Tucana III shows clear evidence of being actively disrupted (Li et al. 2018b).

4 CAVEATS AND SOLUTIONS

4.1 Large Magellanic Cloud bias

One of the key components in understanding the present-day dwarf population of the Milky Way has been contributions from DES. DES has revealed a large number of ultrafaint galaxies in the vicinity of the sky near the Large Magellanic Coud (LMC), which immediately leads to the question of whether most, if not all, of these ultrafaint galaxies fell in with the LMC. This scenario is not difficult to imagine, as LMC-mass haloes could easily host tens of ultrafaint dwarf satellites themselves (Deason et al. 2015; Dooley et al. 2017). Several works have investigated which of the DES dwarfs can reasonably be associated with the LMC. For example, Sales et al. (2017) suggest that of the DES dwarfs within 50 kpc, only Tucana IV can be potentially associated with the LMC. However, Jethwa, Erkal & Belokurov (2016) suggest that three of the DES dwarfs within 50 kpc can be reasonably associated with the LMC, with Tucana III having a $\geq$ 50 per cent probability of being associated with the LMC, and Reticulum II and Tucana IV having a $\geq$ 70 per cent probability of association.

Five of the 18 dwarf galaxies within 50 kpc of the Milky Way were discovered in DES fields. If we assume that all of these are associated with the LMC and therefore are not fairly compared to our simulations (none of which have an LMC-like system at a similar distance), we can compare our expectations to a total of 13 non-LMC dwarfs. From Fig. 2, we see that this would allow us to more easily populate only $V_{peak} > 10$ km s^{-1} dwarfs with galaxies. These are still below the atomic cooling limit, but not as drastically as those in the preferred models discussed above. If the LMC is indeed this critical to a full understanding of the satellite population of the Milky Way, this justifies a dedicated programme to simulate Milky Way haloes with targeted LMC-like subhaloes in the future.

4.2 Numerical disruption

Another potential explanation for the low-mass scale required to explain the radial distribution of satellites is that subhalo disruption at small radii is dominated by numerical error. If a factor of $\sim$5 more $V_{peak} \simeq 20$ km s^{-1} subhaloes survive at small radii than we are capturing, then the primary concern would go away. While our simulations pass basic convergence tests in the presence of disc potentials down to masses $\sim$1000 times smaller than this V_{peak} value (see Garrison-Kimmel et al. 2017, who have slightly worse resolution than our simulations). Additional evidence of numerical disruption would be if the convergence of our V_{peak} functions (Fig. 1) is worse in the inner regions of the Milky Way. We present a more complete analysis of the convergence of the simulations in the Appendix.

There is a fairly extensive body of literature suggesting that cuspy dark matter haloes are never completely disrupted and that a tiny cusp always survives even if systems lose >99 per cent of their initial mass (Goerdt et al. 2007; Peñarrubia et al. 2010; van den Bosch et al. 2018). Of particular relevance in determining if our simulations could be subject to substantial numerical disruption is the work of van den Bosch & Ogiya (2018). They suggest that many haloes are artificially disrupted at far higher halo masses than would be naively assumed by convergence studies of halo mass functions (which is how we set our resolution in this work). They also provide criteria for determining if a subhalo is safe from the effects of numerical disruption. For a circular orbit at 10 per cent of the virial radius, a subhalo needs to be simulated with about 10^6 particles and a softening length of 0.003 times the scale radius of the subhalo. These criteria vary strongly with the tidal field the subhalo experiences.

The criteria suggested in van den Bosch & Ogiya (2018) would place the mass resolution for our simulations at $V_{peak} \simeq 30$ km s^{-1}. We identify a severe discrepancy with the conventional reionization threshold at a V_{peak} value only slightly smaller this, but the tidal field should be even stronger in the disc simulations, so the resolution criteria may be even more restrictive.

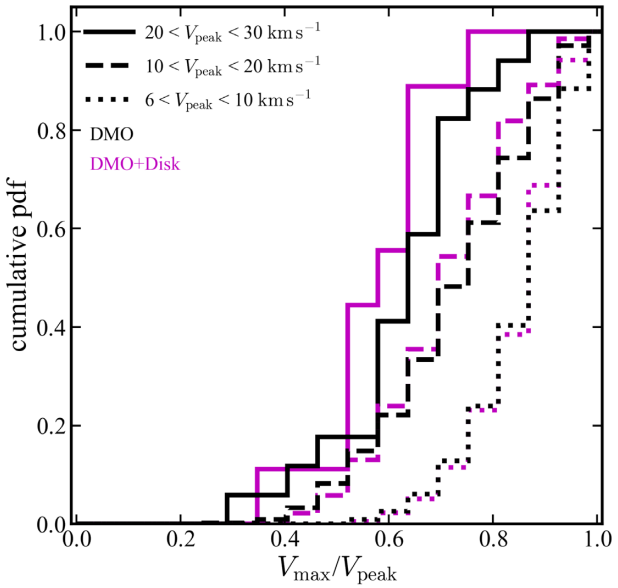

Figure 6. The effect of stripping on surviving subhaloes from both the dmo (black) and disc (magenta) simulations, represented as the ratio between present day V_{max} and V_{peak}. The different line styles represent different bins in V_{peak}. Interestingly, the stripping is only different in the highest-mass bin, for subhaloes between 20 and 30 km s^{-1}. However, the stripping is similar for the dmo and disc runs in other mass bins. Note that our resolution limit does not allow us to capture subhaloes much smaller than $V_{max} = 4.5$ km s^{-1}, which explains why the higher mass subhalo bins can be tracked to smaller V_{max}/V_{peak} ratios.

A related question is by how much our surviving subhaloes are stripped after infall. We explore this in Fig. 6, where we plot the differences in stripping for the surviving haloes in both the dmo and dmo+disc simulations within 50 kpc. Interestingly, the only difference between the two sets of simulations is seen in the highest mass bin (20 km s^{-1} to 30 km s^{-1}), where subhaloes in the disc simulation are stripped on average 5 per cent more than in the dmo simulations. For subhaloes with $V_{peak} \leq 20$ km s^{-1}, the difference in stripping between the dmo and disc simulations is much smaller, just about 1 per cent on average. This implies that the disc is causing significant damage to these subhaloes, driving their masses below our resolution limit, rather than simply lowering their masses and allowing them to survive. After their masses drop below our resolution limit, they are 'destroyed' in our catalogues only because we cannot track them anymore. This means that haloes in the $V_{peak} =$ 10–20 km s^{-1} range will drop out of our catalogues at $V_{max}/V_{peak} \approx$ 0.3, which is roughly where the relevant histogram in Fig. 6 drops to zero, and will be subjected to 90 per cent to 99 per cent mass-loss from stripping. There is no indication that the high-mass group of haloes (solid lines) has a tail that is boosted with respect to the lower mass bins (dashed), as might be expected if there was a catastrophic numerical threshold at $V_{peak} \simeq 20$ km s^{-1}, potentially indicating that our simulations are not subject to numerical disruption above our assumed completeness. However, we stress that more work is needed to understand the results of van den Bosch & Ogiya (2018) in the context of cosmological simulations of the kind employed here.

One possible way to alleviate potential issues with numerical disruption is to include orphan satellites. In such a simulation, satellites that are disrupted are instead replaced with a semi-analytic model that tracks the disrupted subhaloes below the nominal resolution of the simulation, and tracks how they are stripped, and their positions. Such an approach was followed by Nadler et al. (2018) who investigated the galaxy–halo connection for satellites of the Milky Way. They then compute a threshold for galaxy formation as a part of their model. They find that even with the inclusion of orphan haloes, their model prefers a minimum halo mass for galaxy formation between $\log(M_{min}/M_\odot) = 7.5$ and 8.1, which roughly corresponds to halo circular velocities between 7 and 10.7 km s^{-1}, still much lower than the canonical galaxy formation cut-off

4.3 Star formation in low-mass haloes

Another option is that galaxies are indeed forming in haloes that are lower mass than conventional models have suggested. If this is the case, star formation in local ultrafaint dwarfs could have proceeded by molecular cooling, as expected for Pop III formation in mini-haloes (Bromm & Larson 2004; Bland-Hawthorn, Sutherland & Webster 2015). If the temperature distributions presented in Fig. 4 reflect a physical reality, ultrafaint galaxies must form in the kind of haloes usually associated with the first stars.

Another possibility is that reionization happened later than is often assumed in the volume surrounding the Milky Way. Naively, we expect star formation to proceed in galaxies at high redshift if they have circular velocities above the atomic cooling scale prior to reionization $V_{max} > 16$ km s^{-1}. After reionization, star formation is assumed to shut down unless the halo is above the suppression scale (typically 20–30 km s^{-1}; see Fitts et al. 2017 for a recent discussion). If reionization happened late, we would have more small haloes in place earlier, perhaps increasing the global likelihood for galaxy formation at a fixed halo mass.

Recently, cosmological simulations of galaxy formation in very small haloes have begun to see star formation in very small haloes. For example, Wheeler et al. (2018) ran ultra-high resolution simulations of ultrafaint dwarf galaxy haloes (gas particle masses of 30 $M_\odot$) and found that star formation occurs in every halo with $M_{halo} \geq 10^{8.6}$ $M_\odot$ ($V_{max} \geq 12$ km s^{-1}), below the canonical threshold for galaxy formation. Additionally, Munshi et al. (2018) have used ChaNGa simulations to show that the relationship between haloes and galaxies at very low masses is sensitive to the specifics of the star formation model adopted. Specifically, they run simulations with a metal-line cooling model and a H_2-based subgrid model. These models see large differences in the number of occupied haloes, with the metal cooling simulation forming a factor of 5 more ultrafaint-like galaxies, which form in haloes down to 10^7 $M_\odot$. The difference is due to the density threshold at which star formation occurs in the two simulations, with the metal cooling simulations allowing gas in haloes to become denser prior to reionization. While several state-of-the-art simulations have shown that galaxy properties are insensitive to the adopted star formation threshold (see Hopkins et al. 2018 and references therein), this is only true in larger galaxies where star formation self-regulates via feedback. In the smallest haloes ($V_{peak} \lesssim 20$ km s^{-1}), star formation is regulated by the external ionizing field and thus can be more sensitive to adopted threshold (Munshi et al. 2018). Future work in this direction may provide important physical insights into how we might naturally form faint galaxies in $V_{peak} \simeq 6$–10 km s^{-1} haloes.

5 CONCLUSION

In this work, we utilized a new suite of 12 cosmological simulations of Milky Way-like haloes that include a central disc potential (Kelley et al. 2019). The haloes were chosen to match the mass of the Milky Way ($M_{\rm vir} = 0.8–2 \times 10^{12}$ M$_\odot$). The galaxy is modelled as an evolving disc+bulge potential that grows to match the Milky Way at $z = 0$. The inclusion of the galaxy drastically affects the subhalo abundance at small radii, as shown in Fig. 1, which is consistent with past work based on hydrodynamic simulations (Brooks & Zolotov 2014; Wetzel et al. 2016; Zhu et al. 2016; Garrison-Kimmel et al. 2017; Graus et al. 2018).

We compared the subhalo distributions at small radius to the current census of galaxies that exist within 50 kpc of the Milky Way disc, most of which are ultrafaint galaxies discovered in digital sky surveys (e.g. Willman et al. 2005; Zucker et al. 2006; Drlica-Wagner et al. 2015; Koposov et al. 2018). Even though our census of small galaxies is likely incomplete, we require very low-mass haloes to host galaxies in order account for all of the presently known galaxies (see Fig. 2). In particular, we need haloes as small as $V_{\rm peak} = 6\,{\rm km\,s^{-1}}$ to host ultrafaint galaxies. These systems have virial temperatures as low as ∼1500 K, which is not only well below the typical scale where reionization is expected to suppress galaxy formation ($V_{\rm peak} \simeq 20\,{\rm km\,s^{-1}}$ and $T_{\rm vir} \simeq 15\,000$ K) but also much smaller than the atomic cooling limit ($V_{\rm peak} \simeq 16\,{\rm km\,s^{-1}}$ and $T_{\rm vir} = 10\,000$ K).

We explored these results by mock-observing our Milky Way haloes over regions that mimic DES and SDSS fields using toy models that allow the fraction of haloes that host galaxies to vary from 0 to 1 at a characteristic $V_{\rm peak}$ scale. As shown in Fig. 4, the models that work populate haloes with $V_{\rm peak}$ values between 6 and 16 $\rm km\,s^{-1}$ ($T_{\rm vir} = 1500–10\,000$ K), much smaller than would be conventionally expected. It is important to note that any new discoveries of ultrafaint dwarf galaxies close to the Milky Way would only increase the need to populate very small haloes with galaxies.

There are at least three possibilities that could change these conclusions. First, several of the ultrafaint 'galaxies' we include in our analysis (Table 1) could be misclassified star clusters. Ultrafaint galaxies are differentiated from star clusters by inhabiting dark matter haloes (Willman & Strader 2012). If some fraction of the satellites in our comparison do not have dark haloes then the implied threshold $V_{\rm peak}$ for galaxy formation would increase accordingly.

A second possibility is that many, if not most dwarfs that were discovered by DES were brought in with the LMC. If this is the case, it would bias the Milky Way dwarf population to be overabundant compared to what is typical for haloes of the Milky Way's mass. Of the 18 total dwarf galaxies within 50 kpc of the Milky Way, five were discovered in DES. Fig. 2 shows that if all five of these were removed from the comparison the need to populate very low-mass subhaloes would be lessened, but that there would still be tension unless we allow for most $V_{\rm peak} \simeq 10\,{\rm km\,s^{-1}}$ haloes to host galaxies. Even in this fairly conservative scenario (which ignores sky coverage incompleteness) we require galaxy formation below the atomic cooling limit.

A third possibility is that much of the destruction we see is a numerical artefact (van den Bosch et al. 2018). By conventional convergence-test standards, we appear to be well resolved down to $V_{\rm peak} = 6\,{\rm km\,s^{-1}}$ and certainly to $V_{\rm peak} = 10\,{\rm km\,s^{-1}}$; however, by the criteria described in van den Bosch & Ogiya (2018), we could be affected by numerical issues at the critical scale $V_{\rm peak} = 20\,{\rm km\,s^{-1}}$. If so, then ultrafaint galaxies may reside within haloes with $V_{\rm peak}$ above the canonical reionization suppression scale, and the numerical challenge facing Milky Way satellite modellers will become quite significant.

Aside from the caveats discussed above, our results suggest that haloes well below the atomic cooling limit host ultrafaint galaxies. One implication of such a scenario is that we would expect ∼1000 such systems within 300 kpc of the Milky Way (see the left-hand panel of Fig. 1 at $V_{\rm peak} \simeq 7\,{\rm km\,s^{-1}}$ and the last row of Table 1 in Kim et al. 2018). This count will be testable with LSST and is significantly higher than previous completeness-correction estimates, which had relied on dark matter only simulations. Whatever the answer, the results presented here motivate renewed efforts to understand galaxy formation in the smallest haloes and the effect of the near-field environment on their evolution.

ACKNOWLEDGEMENTS

The authors would like to thank Josh Simon for providing the dispersion velocities of dwarf satellites used in this work, and Alyson Brooks, Alex Drlica-Wagner, and Denis Erkal for useful discussions. We also thank the anonymous referee for their helpful comments on the manuscript. ASG, TK, CQ, and JSB were supported by NSF AST-1518291, HST-AR-14282, and HST-AR-13888. MBK acknowledges support from NSF grant AST-1517226 and CAREER grant AST-1752913 and from NASA grants NNX17AG29G and HST-AR-13888, HST-AR-13896, HST-AR-14282, HST-AR-14554, HST-AR-15006, HST-GO-12914, and HST-GO-14191 from the Space Telescope Science Institute, which is operated by AURA, Inc., under NASA contract NAS5-26555. Support for SGK was provided by NASA through the Einstein Postdoctoral Fellowship grant number PF5-160136 awarded by the Chandra X-ray Center, which is operated by the Smithsonian Astrophysical Observatory for NASA under contract NAS8-03060. This work used computational resources of the Texas Advanced Computing Center (TACC; http://www.tacc.utexas.edu), the NASA Advanced Supercomputing (NAS) Division and the NASA Center for Climate Simulation (NCCS), and the Extreme Science and Engineering Discovery Environment (XSEDE), which is supported by National Science Foundation grant number OCI-1053575.

REFERENCES

Behroozi P. S., Wechsler R. H., Wu H.-Y., 2013, ApJ, 762, 109
Behroozi P. S., Wechsler R. H., Lu Y., Hahn O., Busha M. T., Klypin A., Primack J. R., 2014, ApJ, 787, 156
Bellazzini M. et al., 2008, AJ, 136, 1147
Belokurov V. et al., 2007, ApJ, 654, 897
Belokurov V. et al., 2009, MNRAS, 397, 1748
Benítez-Llambay A. et al., 2017, MNRAS, 465, 3913
Benson A. J., Frenk C. S., Lacey C. G., Baugh C. M., Cole S., 2002, MNRAS, 333, 177
Bland-Hawthorn J., Gerhard O., 2016, ARA&A, 54, 529
Bland-Hawthorn J., Sutherland R., Webster D., 2015, ApJ, 807, 154
Bovill M. S., Ricotti M., 2009, ApJ, 693, 1859
Boylan-Kolchin M., Bullock J. S., Kaplinghat M., 2011, MNRAS, 415, L40
Bromm V., Larson R. B., 2004, ARA&A, 42, 79
Brooks A. M., Zolotov A., 2014, ApJ, 786, 87
Brown T. M. et al., 2014, ApJ, 796, 91
Bullock J. S., Kravtsov A. V., Weinberg D. H., 2000, ApJ, 539, 517
D'Onghia E., Springel V., Hernquist L., Keres D., 2010, ApJ, 709, 1138
Deason A. J., Wetzel A. R., Garrison-Kimmel S., Belokurov V., 2015, MNRAS, 453, 3568

Despali G., Vegetti S., 2017, MNRAS, 469, 1997
Dooley G. A., Peter A. H. G., Carlin J. L., Frebel A., Bechtol K., Willman B., 2017, MNRAS, 472, 1060
Drlica-Wagner A. et al., 2015, ApJ, 813, 109
Drlica-Wagner A. et al., 2016, ApJ, 833, L5
Efstathiou G., 1992, MNRAS, 256, 43P
Fattahi A., Navarro J. F., Frenk C. S., Oman K. A., Sawala T., Schaller M., 2018, MNRAS, 476, 3816
Fitts A. et al., 2017, MNRAS, 471, 3547
Fitts A. et al., 2018, MNRAS, 479, 319
Garrison-Kimmel S. et al., 2017, MNRAS, 471, 1709
Garrison-Kimmel S., Boylan-Kolchin M., Bullock J. S., Kirby E. N., 2014, MNRAS, 444, 222
Gnedin N. Y., 2000, ApJ, 542, 535
Goerdt T., Gnedin O. Y., Moore B., Diemand J., Stadel J., 2007, MNRAS, 375, 191
Graus A. S., Bullock J. S., Boylan-Kolchin M., Nierenberg A. M., 2018, MNRAS, 480, 1322
Hahn O., Abel T., 2011, MNRAS, 415, 2101
Hernquist L., 1990, ApJ, 356, 359
Hoeft M., Yepes G., Gottlöber S., Springel V., 2006, MNRAS, 371, 401
Hopkins P. F. et al., 2018, MNRAS, 480, 800
Hopkins P. F., 2015, MNRAS, 450, 53
Ibata N. G., Ibata R. A., Famaey B., Lewis G. F., 2014, Nature, 511, 563
Jethwa P., Erkal D., Belokurov V., 2016, MNRAS, 461, 2212
Jethwa P., Erkal D., Belokurov V., 2018, MNRAS, 473, 2060
Katz N., White S. D. M., 1993, ApJ, 412, 455
Kelley T., Bullock J. S., Garrison-Kimmel S., Boylan-Kolchin M., Pawlowski M. S., Graus A. S., 2019, MNRAS, 487, 4409,
Kim S. Y., Peter A. H. G., Hargis J. R., 2017, PRL, 121, 21
Kirby E. N., Boylan-Kolchin M., Cohen J. G., Geha M., Bullock J. S., Kaplinghat M., 2013, ApJ, 770, 16
Kirby E. N., Cohen J. G., Simon J. D., Guhathakurta P., Thygesen A. O., Duggan G. E., 2017, ApJ, 838, 83
Klypin A., Kravtsov A. V., Valenzuela O., Prada F., 1999, ApJ, 522, 82
Koch A. et al., 2009, ApJ, 690, 453
Koposov S. E., et al., 2018, MNRAS, 479, 5343
Koposov S. E., Belokurov V., Torrealba G., Evans N. W., 2015, ApJ, 805, 130
Laevens B. P. M. et al., 2015a, ApJ, 802, L18
Laevens B. P. M. et al., 2015b, ApJ, 813, 44
Li M., Gao L., Wang J., 2019, MNRAS, 483, 2000
Li T. S. et al., 2018a, ApJ, 857, 145
Li T. S. et al., 2018b, ApJ, 866, 22
Longeard N. et al., 2018, MNRAS, 480, 2609
Luque E. et al., 2017, MNRAS, 468, 97
Macciò A. V., Frings J., Buck T., Penzo C., Dutton A. A., Blank M., Obreja A., 2017, MNRAS, 472, 2356
McMillan P. J., 2017, MNRAS, 465, 76
McQuinn M., 2016, ARA&A, 54, 313
Miyamoto M., Nagai R., 1975, PASJ, 27, 533
Moore B., Ghigna S., Governato F., Lake G., Quinn T., Stadel J., Tozzi P., 1999, ApJ, 524, L19
Munshi F., Brooks A. M., Applebaum E., Weisz D. R., Governato F., Quinn T. R., 2017, preprint (arXiv:1705.06286)
Munshi F., Brooks A. M., Christensen C., Applebaum E., Holley-Bockelmann K., Quinn T. R., Wadsley J., 2018, AJ, 874, 40
Nadler E. O., Mao Y.-Y., Green G. M., Wechsler R. H., 2018, AJ, 873, 34
Newton O., Cautun M., Jenkins A., Frenk C. S., Helly J. C., 2018, MNRAS, 479, 2853
Ocvirk P. et al., 2016, MNRAS, 463, 1462
Okamoto T., Gao L., Theuns T., 2008, MNRAS, 390, 920
Oñorbe J., Garrison-Kimmel S., Maller A. H., Bullock J. S., Rocha M., Hahn O., 2014, MNRAS, 437, 1894
Oñorbe J., Hennawi J. F., Lukić Z., 2017, ApJ, 837, 106
Peñarrubia J., Benson A. J., Walker M. G., Gilmore G., McConnachie A. W., Mayer L., 2010, MNRAS, 406, 1290
Planck Collaboration et al., 2016, A&A, 594, A13
Popping G. et al., 2015, MNRAS, 454, 2258
Read J. I., Erkal D., 2019, MNRAS
Riley A. H. et al., 2019, MNRAS, 486, 2679
Rodriguez Wimberly M. K., Cooper M. C., Fillingham S. P., Boylan-Kolchin M., Bullock J. S., Garrison-Kimmel S., 2019, MNRAS, 483, 4031
Sales L. V., Navarro J. F., Kallivayalil N., Frenk C. S., 2017, MNRAS, 465, 1879
Sawala T. et al., 2016, MNRAS, 456, 85
Simon J. D. et al., 2011, ApJ, 733, 46
Simon J. D. et al., 2015, ApJ, 808, 95
Simon J. D. et al., 2017, ApJ, 838, 11
Simon J. D., 2019, preprint (arXiv:e-print)
Simon J. D., Geha M., 2007, ApJ, 670, 313
Smith R., Flynn C., Candlish G. N., Fellhauer M., Gibson B. K., 2015, MNRAS, 448, 2934
Somerville R. S., 2002, ApJ, 572, L23
Springel V., 2005, MNRAS, 364, 1105
Thoul A. A., Weinberg D. H., 1996, ApJ, 465, 608
Tollerud E. J., Bullock J. S., Strigari L. E., Willman B., 2008, ApJ, 688, 277
Torrealba G. et al., 2018, MNRAS, 475, 5085
van den Bosch F. C., Ogiya G., 2018, MNRAS, 475, 4066
van den Bosch F. C., Ogiya G., Hahn O., Burkert A., 2018, MNRAS, 474, 3043
van der Wel A. et al., 2014, ApJ, 788, 28
Walsh S. M., Jerjen H., Willman B., 2007, ApJ, 662, L83
Weisz D. R., Dolphin A. E., Skillman E. D., Holtzman J., Gilbert K. M., Dalcanton J. J., Williams B. F., 2014, ApJ, 789, 147
Wetzel A. R., Hopkins P. F., Kim J.-h., Faucher-Giguère C.-A., Kereš D., Quataert E., 2016, ApJ, 827, L23
Wheeler C. et al., 2018, preprint (arXiv:e-print)
Wheeler C., Oñorbe J., Bullock J. S., Boylan-Kolchin M., Elbert O. D., Garrison-Kimmel S., Hopkins P. F., Kereš D., 2015, MNRAS, 453, 1305
Willman B. et al., 2005, AJ, 129, 2692
Willman B., 2010, Adv. Astron., 2010, 285454
Willman B., Strader J., 2012, AJ, 144, 76
Willman B., Geha M., Strader J., Strigari L. E., Simon J. D., Kirby E., Ho N., Warres A., 2011, AJ, 142, 128
Zhu Q., Marinacci F., Maji M., Li Y., Springel V., Hernquist L., 2016, MNRAS, 458, 1559
Zucker D. B. et al., 2006, ApJ, 650, L41

APPENDIX: RESOLUTION TESTS

Here, we describe the resolution tests for the simulations presented in this work. From our suite of simulations, we have resimulated one system at 8 and 64 times lower resolution, corresponding to particle masses of 2.3×10^5 $M_\odot$ and 1.85×10^6 $M_\odot$. We simulated these systems in an identical manner to our highest resolution simulation, by first simulating the system from $z = 100$ to $z = 0$ in dark matter only. Then resimulating the system from $z = 3$ with the added disc potential. In this case, we used a potential with the exact same properties and evolution as the system in our fiducial run of the simulation. We refer to the different resolutions, from lowest resolution to our highest resolution as z11, z12, and z13. With the z13 simulation being the fiducial resolution used throughout the paper.

In order to estimate the effect of resolution on our results, we calculate the differential $V_{\rm peak}$ function and differential radial distribution of satellites. As we only have one system simulated at lower resolution, we have attempted to account for potential variations in the satellite distributions between runs by averaging over the most recent 14 snapshots of the simulation (this corresponds to evolution from $z = 0.1$ to $z = 0$). The results of this analysis can be seen in Figs A1 and A2. In Fig. A1, we present the differential

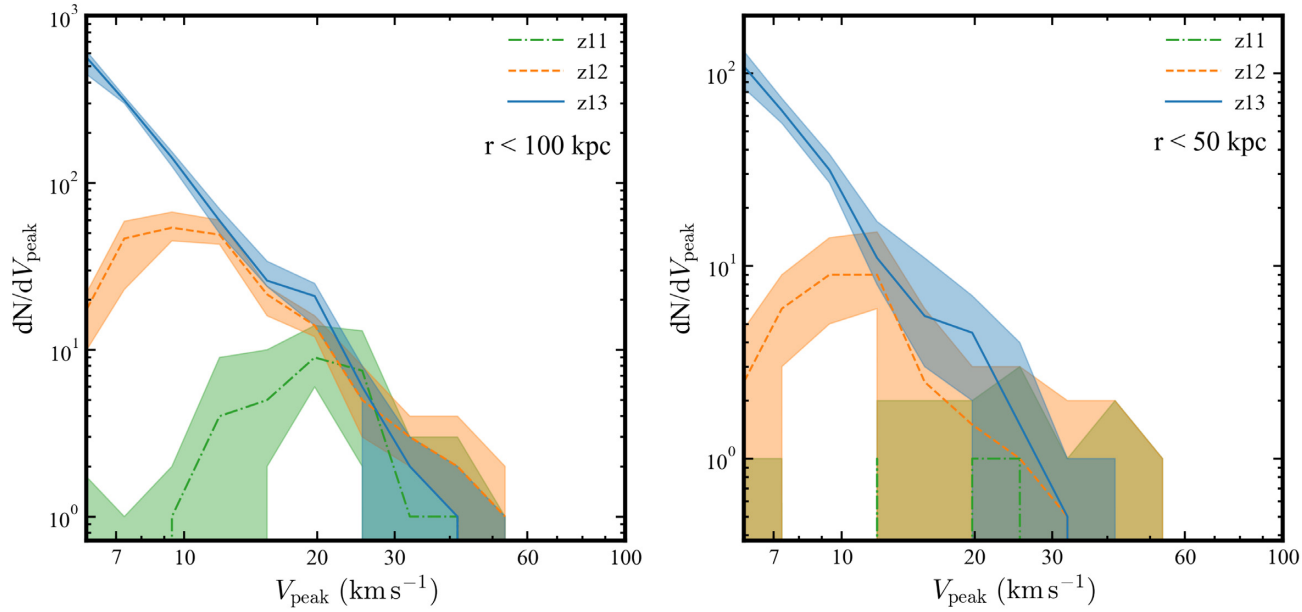

Figure A1. Differential $V_{\rm peak}$ function for the same simulated halo at three different resolutions simulated in the disc configuration. The left-hand and right-hand panels show the $V_{\rm peak}$ functions for all subhaloes within 100 kpc (left) and 50 kpc (right). The shaded regions represent the minimum and maximum of the $V_{\rm peak}$ functions during the last 14 snapshots of the simulation (representing a redshift range of $z = 0.1$–0) in order to account for differences in subhalo orbits between reruns of the simulation at different resolutions, and the line represents the median of the distributions.

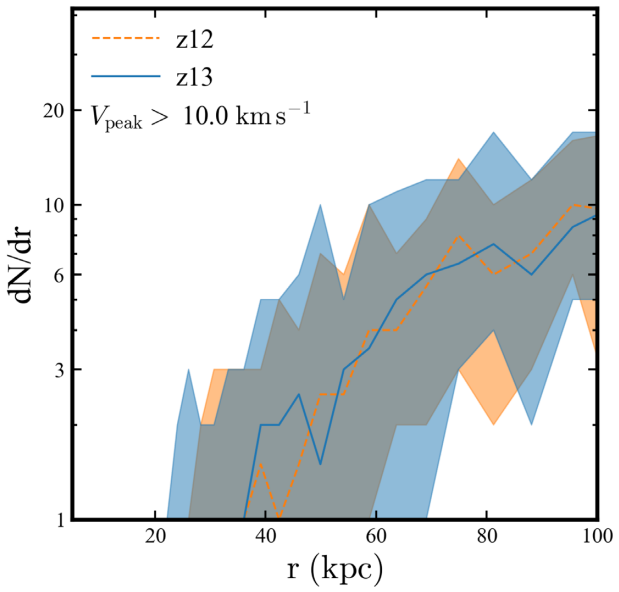

Figure A2. The differential radial distribution of satellites within 100 kpc for our resolution test. The figure shows all haloes above the resolution limit of our intermediate resolution (z12) run ($V_{\rm peak} > 10\ {\rm km\,s^{-1}}$). As in Fig. A1 the subhalo distributions are converged for $V_{\rm peak} > 10\ {\rm km\,s^{-1}}$ to the point where we completely run out of subhaloes, and well within 50 kpc. Once again, the simulations were run at all resolutions in the disc configuration.

$V_{\rm peak}$ distributions for the three runs at two different radii, 50 and 100 kpc, and in Fig. A2, we present the radial distributions out to 100 kpc for the z12 and z13 runs, showing all haloes with a $V_{\rm peak} > 10\,{\rm km\,s^{-1}}$ (the resolution of the z12 run).

From these experiments, it is clear that the simulations appear to be converged to the assumed completeness of $V_{\rm peak} = 6\ {\rm km\,s^{-1}}$ for the z13 runs within 50 kpc. This result differs from that found in some other works including the appendix of Newton et al. (2018) where they compared the radial distribution of satellites with $V_{\rm peak} \geq 10\ {\rm km\,s^{-1}}$ in the Aquarius A-1 and A-2 simulations, and found that the higher resolution simulation (A-1) had more subhaloes at smaller radii with the effect persisting out to the virial radius. The Aquarius A-1 simulation is higher resolution than the highest resolution simulation used in this work. This potentially points to higher resolution subhaloes being more resistant to the tidal forces of the disc potential. The difference between these two works could also be the result of other differences between the simulations such as softening lengths or halo finding techniques.

This paper has been typeset from a TEX/LATEX file prepared by the author.